Charge and mass distributions in the reaction of ^{40}Ar ions with ^{238}U†

J. V. Kratz,† J. O. Liljenzin,‡ A. E. Norris,§ and G. T. Seaborg
Lawrence Berkeley Laboratory and Department of Chemistry, University of California, Berkeley, California 94720
(Received 8 December 1975)

The reaction of 288 MeV ^{40}Ar ions with thick ^{238}U targets has been studied experimentally with nuclear chemistry techniques. The formation cross sections of 130 radioactive nuclides were measured. The data have been used to delineate charge and mass distributions. The mass distribution is interpreted as a superposition of several components: transfer products (quasielastic component, 400±120 mb), multinucleon transfer products (deep inelastic component, 100±50 mb) and products from complete fusion-fission (620±150 mb). In addition, there is evidence for sequential fission of heavy products formed in quasielastic and deep inelastic transfer reactions. In the first case a double-humped mass distribution (150±30 mb) with the characteristics of low-energy fission is observed. Apparently, the sequential fission after deep inelastic processes occurs at higher excitation energies. For the quasielastic component the mass to charge ratio is close to that of the projectile or target, whereas for the deep inelastic component and for the fusion-fission component the mass to charge ratios appear to be fully equilibrated. Proton pickup reactions in the deep inelastic reactions of ^{40}Ar lead to a buildup of products up to at least $Z = 26$, indicating a continuous development from deep inelastic transfer to fusion-fission.

[NUCLEAR REACTIONS ^{238}U+^{40}Ar, $E \leq 288$ MeV; measured $\sigma(Z,A)$; deduced charge and mass distributions, σ for quasielastic transfer, deep inelastic transfer, fusion-fission, σ_r, l.]

I. INTRODUCTION

Evaluations of complete fusion cross sections[1] in heavy-ion interactions of ^{40}Ar ions and heavier projectiles with medium and heavy tragets have shown that the formation of a compound nucleus (including the somewhat more general phenomenon of "complete fusion") is not the most probable reaction channel. Instead, transfer reactions and deep inelastic processes contribute more significantly than is the case for lighter systems. The experimental evidence available at present was obtained by various techniques developed and applied for the detailed investigation of specific reaction channels. Fusion cross sections were measured with mica track detectors[2] and with $\Delta E, E$ counter telescopes[3]; the kinematic coincidence technique designed to study reactions where two fragments are emitted in the exit channel has been applied to complete fusion-fission[4,5] and to deep inelastic reactions[5-8]; magnetic analysis and/or $\Delta E, E$ methods[9,10] were applied to quasielastic and deep inelastic transfer reactions, to name a few examples.

The many open questions related to the prediction of the magnitude of the fusion cross sections[11] and to the characteristics of deep inelastic processes make it difficult at present to predict the relative importance of the competing known reaction channels in even heavier colliding systems. Also, it cannot be excluded that hitherto unobserved reaction mechanisms become important.

In view of the sometimes highly specialized applications of the above mentioned techniques and in view of the large uncertainties in predicting cross sections for very heavy systems, the authors felt the need for a survey experiment based on a technique that is equally sensitive to all competing reaction channels. In this paper we report on such a survey experiment. The approach consists of the radiochemical measurement of a large number of integral cross sections of radioactive products produced in the bombardment of an infinitely thick target. Advantages of this approach are the small beam times required—typically an intense 1–2 h bombardment is sufficient to measure cross sections of more than one hundred reaction products—and the fact that cross sections are obtained for products uniquely characterized in Z and A without the need for assumptions about the reaction mechanism.

The reaction system investigated in this work is that of 288 MeV ^{40}Ar ions impinging on ^{238}U. The results are compared with data obtained in kinematic coincidence experiments with this reaction that have been reported by others.[5] It appears likely that the properties of the product cross-section distribution for light products ($Z \leq 26$) observed in the reaction[10,12] of ^{40}Ar with ^{232}Th can be compared with the radiochemical results for ^{40}Ar on ^{238}U.

Besides the determination of the cross sections for complete fusion-fission and direct reactions, there are a few other questions to which the pres-

ent work attempts to make some contribution: (1) that of the buildup of products with $Z > 18$ in deep inelastic collisions of ^{40}Ar ions, (2) the question of the charge to mass ratios of the quasielastic transfer, deep inelastic transfer, and complete fusion-fission products, (3) the question of the amount of fission of the moderately excited heavy fragments produced by the transfer of a few nucleons, (4) the amount of sequential fission of the highly excited heavy fragments formed in deep inelastic collisions, and (5) the mass distributions of these two different transfer-induced fission reactions.

A short note on results of the present work was published elsewhere.[13] A parallel study of the reaction of ^{84}Kr with ^{238}U is the subject of a forthcoming paper.[14]

II. METHODS

A. Experimental procedure

1. Irradiations

The experimental irradiations were performed at the Lawrence Berkeley Laboratory heavy-ion linear accelerator (superHILAC). The targets consisted of a stack of two or three uranium metal foils of ~30 mg/cm^2 thickness and natural isotopic composition. A surface layer of uranium oxide was removed from each foil prior to irradiation by etching it with cold concentrated HNO_3 under argon atmosphere. The stack of etched metal foils was clamped against a water-cooled copper block inside a Faraday cup connected to a current integrator which permitted the recording of the beam intensity and the total charge collected. Secondary electron emission was suppressed by an electrostatic field (300 V) and a transverse magnetic field (~500 G). It is known from comparison with elastic scattering cross sections that this cup arrangement gives beam current readings that are accurate to better than 20%. The target foils were irradiated with $^{40}Ar^{13+}$ beams of 288 MeV, beam diameter $\leq$12 mm, with intensities of several hundred nA, typically for 1 or 2 h. After irradiation the first uranium foil was quickly counted without chemical separation to identify short-lived isotopes (e.g., ^{239}U, ^{41}Ar, ^{38,39}Cl, and ^{107}Rh) via prominent γ-ray peaks that could be unambiguously identified in the complex γ-ray spectra. Afterwards this foil was dissolved and separated into several chemical fractions. The thickness of the first foil is sufficient to slow down the ^{40}Ar particles to energies below the Coulomb barrier (this requires 17.3 mg U/cm^2 [15]) and, in addition, to stop the majority of reaction products within the foil. However, quasielastic transfer products such as ^{41}Ar, ^{38,39}Cl, and ^{38}S, comprising 9–12% of the total activities, were also found in the second foil. To determine these percentages the second foil was also processed chemically and assayed for the same radioactive products as the first foil. From the activity of ^{99}Mo, and upper limits for ^{107}Rh, ^{139}Ba, ^{194}Au, and ^{239}Np, it was possible to deduce that none of these reaction products escaped to more than 2% into the second foil. The third uranium foil, which served as a monitor for neutron-induced fission of ^{238}U in the target, was assayed chemically for ^{99}Mo. In this way, the contribution of neutron-induced fission to the yields of neutron-rich isotopes in the mass range $80 \leq A \leq 150$ was shown to be about 1%. The stacked foil targets disintegrated if the ^{40}Ar beam intensities exceeded 300 nA. Therefore, for a 2 μA bombardment a single 25 mg/cm^2 thick uranium layer sputtered onto an aluminum backing was used. Small Ar impurities in this target originating from the sputtering process did not affect the Au, Tl, lanthanide, and Y yields that were measured in this experiment.

2. Chemical separations

The chemical procedure for processing heavy-ion bombarded uranium targets was described in a previous publication.[16] Originally, this procedure was developed to isolate a superheavy element fraction by taking advantage of the predicted strong tendency of these elements to form bromide complex ions. By adding further separation steps, based on the volatility of bromides and the different degrees of complex ion formation in HBr and HCl solutions, the targets were finally separated into a total of seven chemical fractions. For a detailed investigation of the isotopic yield distributions of Y (together with the heavy lanthanides), Au, and Tl isotopes, specific separations for Y and Au+Tl were also applied. These procedures are described in Appendix B.

3. Radioactivity measurements

The activity of each product was determined by observing its characteristic γ-ray transitions. γ-ray spectra were recorded with efficiency-calibrated Ge(Li) diodes of 10 and 50 cm^3 active volume and 3.5 and 2.8 keV resolution at 1332 keV. The photoelectric efficiency of the detectors was determined as a function of γ-ray energy for a number of well defined counting geometries with a set of calibrated sources. The γ-ray spectrum of each sample in the energy range 50 keV $\leq E \leq$2 MeV was measured at about 1 keV/channel as a function of time by a 400 or 4096 channel pulse

height analyzer for a total period of about three weeks.

B. Treatment of data

The spectral data were analyzed with a set of computer programs as described elsewhere.[17] These programs allow the experimenter to use to advantage information "external" to a given γ-ray spectrum, such as the chemical separations occurring in the preparation of the sample, the rate of decay of a γ-ray peak, and available information about parent-daughter decay relationships and the quantal yields of additional γ-ray lines from the decay of the nuclide under consideration. The intensity of each γ ray was displayed as a function of the time of count on an interactive computer console. The decay data were analyzed in terms of the decay characteristics of known nuclides contained in a γ-ray reference table which was compiled from various sources.[18-20] The reference table was broken into subsets consisting of the nuclides that might be present in a given chemical fraction. Thus, the assignment of a γ-ray peak and its intensity (I_γ) to a specific isotope was made on the basis of the chemical fraction in which it was observed, its half-life, γ-ray energy, parent-daughter relations, and corroboration by accompanying γ-ray peaks with the proper energies, half-lives, and intensities.

If necessary, the measured activities were corrected for the variation of the beam intensity with time. Corrections of the activities due to precursor decay were also applied. The absolute values of the cross sections of the products were determined from the corrected activities, the quantum yields (I_γ), the half-life, the chemical yield, effective target thickness (17.3 mg U/cm^2), beam intensity, and irradiation period (for details see Appendix A). If several γ rays of the same isotope were observed, the cross section reported below generally was calculated from the weighted average of all the corrected γ-ray intensities. The estimated errors in computing the absolute values of the cross sections are ±4% for the counting efficiency and ±3% for the chemical yield. In some cases, where elements were split between two chemical fractions,[16] the latter uncertainty could be as large as 10%. Uncertainties in the values of I_γ and in the beam current integration were not taken into account. The uncertainties listed in Table I represent a linear combination of these uncertainties and the statistical uncertainty in the corrected activities obtained in decay-curve analyses.

TABLE I. Cross sections of individual radioactive isotopes produced in the bombardment of a thick ^{238}U target with 288 MeV ^{40}Ar ions.

Nuclide	Half-life	Type of cross section [a]	Bombardment designation	Cross section (mb) σ [b]	$\Delta\sigma$ [c]	Selected value	Weighed average σ	$\Delta\sigma$	Remarks
^{24}Na	15.0 h	2	5U	0.47	0.11				
^{38}S	2.83 h	2	6U	33.8	10.9				
^{38}Cl	37.2 min	1	6U	45.7	18.5				
^{39}Cl	56 min	2	6U	70.8	7.2				
^{41}Ar	1.83 h	2	6U	131.6	15.6				
^{42}K	12.4 h	1	5U	6.56	0.86				
^{43}K	22.2 h	2	5U	6.94	0.69				
^{47}Ca	4.54 day	2	6U	2.54	0.18	x			
^{47}Ca	4.54 day	2	5U	3.08	0.70				
^{47}Sc	3.42 day	1	6U	2.18	0.36				
^{48}Sc	43.7 h	1	6U	1.84	0.53				
^{48}V	15.97 day	1	6U	<4.1					d
^{52}Mn^g	5.7 d	(3)	6U	1.55	0.31				e
^{56}Mn	2.58 h	2	5U	2.11	0.55		2.39	0.33	
^{56}Mn	2.58 h	2	6U	2.59	0.38				
^{61}Co	1.6 h	2	5U	2.78	0.39				
^{65}Ni	2.52 h	2	6U	2.98	0.41				
^{67}Cu	61.9 h	2	6U	2.90	0.70	x			
^{67}Cu	61.9 h	2	5U	3.80	1.57				
^{69}Zn^m	13.9 h	(1)	5U	1.16	0.18		1.27	0.13	
^{69}Zn^m	13.9 h	(1)	6U	1.39	0.20				
^{71}Zn^m	3.9 h	(1)	5U	0.83	0.27		1.02	0.16	
^{71}Zn^m	3.9 h	(1)	6U	1.15	0.18				
^{72}Zn	46.5 h	2	5U	1.63	0.71		1.76	0.37	

TABLE I *(Continued)*

Nuclide	Half-life	Type of cross section [a]	Bombardment designation	Cross section (mb) σ [b]	$\Delta\sigma$ [c]	Selected value	Weighed average σ	$\Delta\sigma$	Remarks
^{72}Zn	46.5 h	2	6U	1.82	0.33				
^{72}Ga	14.1 h	1	5U	1.60	0.21				
^{80}Br^{m}	4.42 h	(1)	5U	0.85	0.26				
^{82}Br	35.34 h	1	5U	1.91	0.33				
^{83}Br	2.4 h	2	5U	6.25	2.04				
^{84}Br^{g}	31.8 m	(2)	5U	1.80	0.33				
^{84}Rb	34.5 d	1	5U	0.81	0.26				
^{86}Rb	18.7 d	1	5U	2.49	1.13				
^{91}Sr	9.5 h	2	5U	7.82	1.12				
^{92}Sr	2.71 h	2	5U	7.99	1.16				
^{85}Y^{g}	4.9 h	(3)	15U	0.05	0.01				d
^{86}Y^{m}	48 m	(1)	15U	0.07	0.02				
^{87}Y^{m}	13 h	(1)	15U	0.24	0.05				
^{87}Y	80.3 h	1	15U	0.20	0.04				
^{88}Y	108 d	1	15U	0.52	0.08				
^{90}Y^{m}	3.19 h	(1)	15U	1.67	0.26				
^{91}Y^{m}	49.7 m	(1)	5U	3.35	0.36				
^{92}Y	3.54 h	1	5U	2.92	0.50				
^{93}Y	10.1 h	2	5U	10.86	1.16				
^{95}Zr	64 d	2	5U	12.66	2.09				
^{97}Zr	16.8 h	2	5U	10.10	3.31				
^{93}Mo^{m}	6.9 h	(1)	5U	0.39	0.33				
^{99}Mo	66.0 h	2	5U	15.19	1.26				
^{94}Tc^{g}	4.9 h	(3)	5U	0.14	0.05				
^{103}Ru	39.3 d	2	5U	15.40	11.08				
^{105}Ru	35.5 h	2	5U	12.27	1.11				
^{107}Rh	22 m	2	5U	6.83	1.30				
^{112}Pd	20.1 h	2	5U	10.07	1.09				
^{106}Ag^{m}	8.3 d	(1)	5U	0.67	0.39				
^{110}Ag^{m}	250.4 d	(1)	5U	2.1	0.25				
^{111}Ag^{g}	7.5 d	2	5U	10.2	4.31				
^{112}Ag	3.12 h	1	5U	6.19	2.63				
^{115}Cd^{g}	53.4 h	(2)	5U	10.1	3.21				
^{117}Cd m + g	3.3 h 2.42 h	(2)	5U	12.0	1.94				
^{111}In	2.83 h	3	5U	0.12	0.04				
^{123}I	13.2 h	3	5U	1.44	0.20				
^{124}I	4.15 d	1	5U	2.08	0.34				
^{125}I	60.1 d	1	5U	2.47	1.0				
^{126}I	13.0 d	1	5U	4.27	0.76				
^{128}I	25 m	1	5U	4.88	1.30				
^{130}I^{g}	12.36 h	(1)	5U	3.31	$^{+1.07}_{-0.44}$				f
^{131}I	8.04 d	(1)	5U	5.84	0.56				g
^{132}I^{m}	84 m	(1)	5U	4.0	1.2				
^{132}I m + g	84 m 2.38 h	1	5U	4.16	0.72	*x*			
^{133}I	20.8 h	(2)	5U	7.35	0.95				h
^{134}I	52 m	1	5U	7.08	0.81				i
^{135}I	6.59 h	2	5U	6.45	0.72				
^{127}Cs	6.25 h	3	5U	1.05	0.23				
^{129}Cs	32.1 h	1	5U	1.95	0.26				
^{132}Cs	6.47 d	1	5U	4.77	1.41				
^{134}Cs^{m}	2.9 h	(1)	5U	2.30	0.31				j
^{136}Cs	13.0 d	1	5U	2.64	0.39				
^{131}Ba	11.5 d	3	5U	1.93	0.28				
^{139}Ba	82.7 m	2	5U	8.57	2.16				

TABLE I *(Continued)*

Nuclide	Half-life	Type of cross section [a]	Bombardment designation	Cross section (mb) σ [b]	$\Delta\sigma$ [c]	Selected value	Weighed average σ	$\Delta\sigma$	Remarks
^{140}Ba	12.8 d	2	5U	6.45	1.02				
^{140}La	40.2 h	1	5U	3.0	0.51				
^{142}La	92.5 m	2	5U	7.60	1.90				
^{139}Ce	137.5 d	3	5U	5.70	1.50				
^{141}Ce	32.5 d	2	5U	9.28	1.30				
^{143}Ce	33.0 h	2	5U	7.40	1.07				
^{149}Nd	1.73 h	2	5U	3.05	0.58				
^{138}Pr^{m}	2.02 h	(1)	5U	1.05	0.42				
^{148}Pm^{m}	41.3 d	(1)	5U	2.8	0.5				d
^{149}Pm	53.1 h	2	5U	5.0	2.35				
^{150}Pm	2.7 h	1	5U	1.25	0.26				d
^{151}Pm	28 h	2	5U	1.65	0.27				d
^{153}Tb	2.34 d	3	15U	0.43	0.29				
^{156}Tb^{g}	5.35 d	(1)	5U	2.65	0.70				
^{155}Dy	9.59 h	3	15U	0.42	0.19				
^{157}Dy	8.1 h	3	5U	1.63	0.25				
^{157}Dy	8.1 h	3	15U	1.49	0.20		1.55	0.07	
^{161}Er	3.1 h	3	15U	0.72	0.34				
^{171}Er	7.5 h	2	15U	0.17	0.04				
^{165}Tm	30.1 h	3	5U	1.50	0.25				
^{165}Tm	30.1 h	3	15U	0.95	0.14		1.15	0.29	
^{167}Tm	9.25 d	3	5U	4.12	0.59				
^{167}Tm	9.25 d	3	15U	2.72	0.42		3.33	0.70	
^{173}Tm	8.2 h	2	15U	0.21	0.07				
^{172}Lu	6.7 d	1	5U	1.87	0.61				
^{175}Hf	70.0 d	(3)	5U	1.89	0.46				
^{187}W	23.8 h	2	5U	0.27	0.12				
^{186}Re^{g}	90.6 h	(1)	5U	0.99	0.78				d
^{183}Os^{g}	14 h	(3)	5U	0.62	0.39				
^{186}Ir^{g}	15.8 h	(3)	5U	0.63	0.11				
^{188}Ir	41.5 h	1	5U	1.78	0.58				
^{190}Ir^{g}	12.1 d	(1)	5U	1.60	0.81				
^{192}Ir^{g}	74 d	(1)	5U	2.15	0.27				d
^{190}Au	42.8 m	1	15U	0.22	0.04				
^{191}Au	3.18 h	1	15U	0.34	0.19				
^{192}Au	5.0 h	1	15U	0.82	0.11				
^{193}Au	17.65 h	1	15U	1.27	0.10				
^{194}Au	39.5 h	1	15U	1.56	0.21				
^{196}Au^{m}	9.7 h	(1)	15U	0.99	0.08				
^{196}Au^{g}	6.2 d	1	15U	1.41	0.11				
^{198}Au^{m}	2.3 d	(1)	15U	>0.27					k
^{199}Au	3.13 d	1	15U	0.15	0.06				
^{200}Au m + g	18.7 h 48.4 m	1	15U	0.026	0.01				
^{198}Tl^{m}	1.87 h	(1)	15U	0.35	0.05				
^{198}Tl	1.87 h 5.3 h	1	15U	0.68	0.07				l
^{199}Tl	7.42 h	1	5U	1.27	0.12				
^{200}Tl	26.1 h	1	15U	1.32	0.54				
^{201}Tl	73.5 h	1	5U	0.96	0.28				
^{198}Pb	2.4 h	3	5U	0.44	0.19				
^{199}Pb^{g}	1.5 h	(3)	5U	0.62	0.26				
^{200}Pb	21.5 h	3	5U	0.99	0.16				
^{201}Pb	9.4 h	1	5U	1.07	0.21				
^{202}Pb^{m}	3.62 h	(1)	5U	1.06	0.17				
^{204}Pb^{m}	67 m	(1)	5U	0.62	0.22				
^{202}Bi	1.8 h	3	5U	0.22	0.07				d

TABLE I *(Continued)*

Nuclide	Half-life	Type of cross section [a]	Bombardment designation	Cross section (mb) σ [b]	$\Delta\sigma$ [c]	Selected value	Weighed average σ	$\Delta\sigma$	Remarks
^{203}Bi	11.76 h	3	5U	1.47	0.49				
^{204}Bi	11.3 h	3	5U	1.85	0.67				
^{224}Ac	2.9 h	1	5U	0.51	0.10				
^{226}Ac	29 h	1	5U	0.24	0.04				
^{234}Th	24.1 d	2	5U	<60.5					m
^{237}U	6.75 d	2	5U	84.7	20.2				
^{237}U	6.75 d	2	6U	109.6	12.3	x			
^{239}U	23.5 m	2	6U	19.7	2.3				
^{240}U	14.1 h	2	5U	1.41	0.88				
^{238}Np	50.8 h	1	5U	4.38	0.93				
^{239}Np	2.35 d	2	5U	38.4	6.6				

[a] 1: independent yield; 2: cumulative yield within a β^--decay chain; 3: cumulative yield within a β^+- or electron-capture-decay chain. For classifications in parentheses see text and the following example: ^{198}Au^m (1): independent yield of isomer; ^{198}Au^g (1): independent yield of ground state; ^{198}Au 1: independent yield of isomeric state plus ground state.

[b] Assumed effective target thickness 17.3 mg U/cm^2 (Ref. 15), corresponding to a general reaction barrier of 200 MeV (lab) (Refs. 11 and 21).

[c] Linear combination of systematic uncertainties and the uncertainties due to counting statistics.

[d] The assignment of the observed activity to this nuclide is uncertain.

[e] Probably formed from an oxygen contamination of the target.

[f] The 9.2 min isomer (84% isomeric transition) was not observed. The upper uncertainty limit takes into account the possibility that 16% of the independent yield of ^{130}I remained undetected.

[g] Not corrected for the growth from 25 min ^{131}Te^g; this value should be considered as an upper limit.

[h] No precursor correction performed because the isomer ratio of ^{133}Te^m to ^{133}Te^g is unknown; this value should be considered as a lower limit.

[i] The 3.8 min isomer (98% isomeric transition) was not observed. The yield of this state is assumed to be included completely in the measured cross section.

[j] The independent yield of ^{134}Cs^m (8^-) is not equal to the total independent yield of ^{134}Cs, because spin and parity are also high (4^+) for the ground state.

[k] The yields of ^{198}Au^m and ^{198}Au^g were not determined because the decay of the 412 keV γ-ray line, which contains contributions from ^{198}Tl^m, ^{198}Tl^g, ^{198}Au^m, and ^{198}Au^g, could not be resolved into its components.

[l] The yield of ^{198}Tl^g, including the contribution from ^{198}Tl^m (55% isomeric transition) was measured to be 0.52 ± 0.05 mb.

[m] Corrected for the activity of ^{234}Th from the α decay of ^{238}U.

III. RESULTS

Table I lists the integral cross sections which were determined in the most intense bombardments. The data from two preceding low-intensity bombardments were in reasonable agreement with these cross sections. However, due to their large statistical uncertainties and due to the less sophisticated data reduction techniques applied in their evaluation, they were considered less reliable and were not taken into account. A few remarks should be added concerning the "type of cross section" in Table I. (1) In the following discussion the terms "formation cross section" and "yield" (both given in mb) are used interchangeably. As in fission studies we distinguish independent yields and cumulative yields. In low-energy fission the cumulative yield of the last member of a β^--decay chain generally represents the total chain yield. In the reactions investigated in the present work both neutron-deficient and neutron-rich isotopes are formed for a broad range of mass numbers, leading to the occurrence of two independently decaying β-decay chains at a given mass number. Thus, for many mass numbers there is no single isotope for which the cumulative cross section is equal to the total cross section at this mass number ("total mass yield"). (2) Some of the classifications in Table I are given in parentheses. This occurs whenever an isomeric state exists besides the ground state, but only one of them was measured, the other one being undetected due to unfavorable half-lives, low quantum yields, or cross sections below the detection limit. The parentheses thus indicate that these cross sections must be considered as lower limits. In practice it turns out that the independent yields of

the high spin states are generally quite close to the total independent yield of a given isotope as interpolated from the charge dispersion systematics. In particular, this seems to be a good working hypothesis in cases where the spin of the undetected state is low. If both states have spins of a few units of $\hbar$, the selectivity for the higher spin state is far less pronounced.

IV. DISCUSSION

A. Cross section isopleths

The independent and cumulative yields from Table I are plotted vs mass number (after particle evaporation) in Fig. 1(a). The apparent scatter in the data in Fig. 1(a) occurs because independent yields, and even many of the cumulative yields, represent only a fraction of the total mass yields. Figure 1(b) is a contour map of the independent yields in a Z-A plane, indicating yield locations relative to the stability line. The structure revealed by the isopleths in Fig. 1(b) indicates that several yield distributions with different charge and mass dispersions, and hence, different origins, are superimposed on each other. The overall distribution is dominated (1) by the high yields (>100 mb) for transfer products near $A = 40$ and $A = 238$ ["rabbit ears," components E and F in Fig. 1(b)] and (2) by a broad fission product distribution centered around $A \approx 133$. As will be discussed in the following paragraphs, this distribution is not a single component, but consists of products from fusion-fission (component A), from fission of heavy products formed by transfer of a few nucleons and small amounts of excitation energy (component B), and from high-energy fission of heavy products from deep inelastic processes (shaded area D). Furthermore, there are neutron-rich products ranging from low Z values up to $Z \approx 26$ or even higher, that are attributed to deep inelastic transfer reactions (component C).

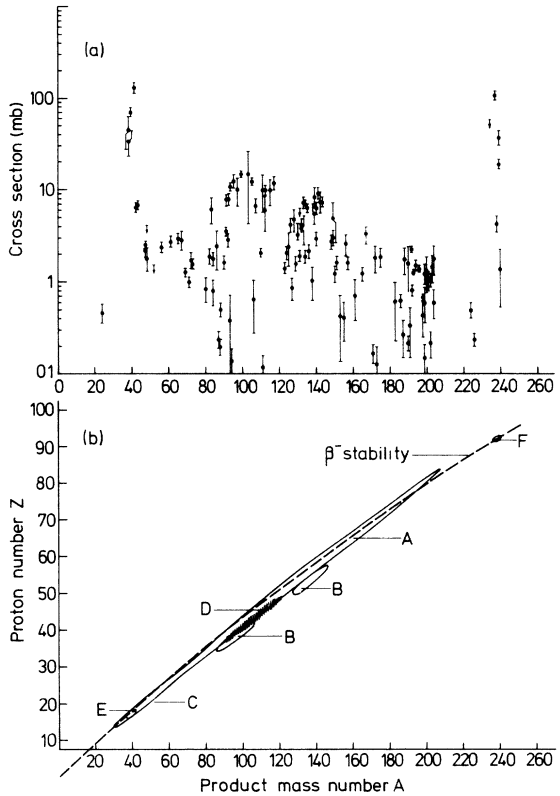

FIG. 1. (a) Independent and cumulative formation cross sections of individual nuclides produced in the bombardment of a thick ^{238}U target with 288 MeV ^{40}Ar ions. (b) Contour lines for equal independent formation cross sections in a Z, A plane. 1 mb isopleths are shown for components A, B, and C. The isopleths for components E and F refer to 10 mb cross sections. For the interpretation of components A through F, see caption of Fig. 5.

B. Charge dispersion curves

For the deduction of the total mass yields from the yields of single isotopes it is necessary that the charge dispersion curve be known for a given mass chain. [In Fig. 1(b) a charge dispersion curve would correspond to a cut through the indicated "yield mountains" at a fixed mass number.] Then the experimentally determined independent or cumulative yield can be related to the total mass yield by correcting for the independent yields of unobserved members of the chain. To arrive at the total mass yield for a given mass one has to integrate the charge dispersion curve; i.e., sum up the independent yields of all isotopes with mass A. We have made the usual assumption regarding the charge distribution originating from a given reaction where two excited fragments are emitted in the exit channel.

Neutrons are emitted from the fragments in a quantity proportional to the fragment mass number:

$$A = A'\left(1 - \frac{\nu}{A_0}\right), \tag{1}$$

where ν is the total number of neutrons per binary event, A' is the mass number of the fission fragment before neutron emission, and A_0 is the composite nucleus mass number. For simplicity, it is assumed that the number of neutrons emitted by an excited fragment of a given mass number is a fixed quantity. It is obvious that the dispersion in the number of neutrons emitted by a fragment is then formally included in the dispersion in the

fragment charge for a given mass number.

For a given fragment mass number A' there exists a most probable nuclear charge $Z_p(A')$ for which the yield of the isobar is highest. The independent yield of an isobar with Z different from Z_p is described by a Gaussian distribution

$$P(Z-Z_p)=P_A\frac{1}{(2\pi\sigma_z^2)^{1/2}}\exp\left(-\frac{(Z-Z_p)^2}{2\sigma_z^2}\right), \quad (2)$$

where σ_z is a parameter describing the width of the isobaric yield distribution for a given A'. The function $Z_p(A')$ was determined both empirically and by using various hypotheses as discussed in Secs. IV C and D. P_A is the mass distribution function (the total mass yield as a function of A'). In agreement with previous experience[22,23] P_A is a Gaussian for complete fusion-fission. If the isobaric dispersions are given by Eq. (2), then the isotopic distribution of an element with the proton number Z has the form

$$P(A'-A'_p) = \frac{P_A}{(\partial Z_p/\partial A')_{A'=A'_p}}\frac{1}{(2\pi\sigma_A^2)^{1/2}}\exp\left(-\frac{(A'-A'_p)^2}{2\sigma_A^2}\right), \quad (3)$$

where A'_p is the most probable mass for a fragment of a given element Z and is determined from the condition $Z_p(A')=Z$.

Corrections for the yields of isotopes not observed experimentally as well as appropriate corrections in determining independent yields from measured cumulative yields depend on the parameters ν, σ_z, $Z_p(A')$ and the function P_A; i.e., on parameters and functions which we are eventually required to find. This situation is further complicated by the fact that we have to deal with the superposition of several yield distributions, especially in the mass region $80 \leq A \leq 150$ [see Fig. 1(b)]. Therefore, to determine the charge dispersion parameters and the mass distribution functions P_A, we had to use successive approximations. The first step in this iterative procedure was the plotting of isotopic distributions [i.e., cuts through the yield mountains in Fig. 1(b) for fixed proton number Z] and the empirical deduction of the above mentioned parameters for the fusion-fission component, followed by appropriate estimates for the other less abundant components.

In plotting isotopic distributions of fission products (after neutron emission) and fitting them with a Gaussian-shaped function, one makes the following simplifications in comparison with Eqs. (1) and (3): the number of neutrons evaporated is assumed to be constant in a small mass range of ≤7 mass units and P_A is assumed to be constant in the same mass interval. Note that the correction introduced to reconstruct the individual yield of certain isotopes is important only for isotopes with Z close

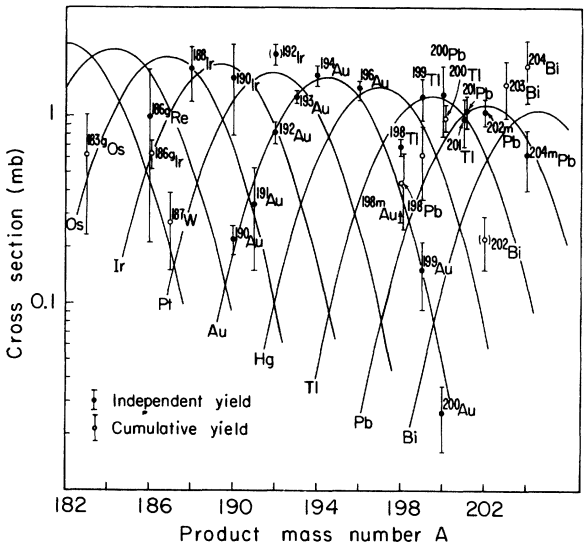

FIG. 2. Independent and cumulative yields of isotopes of the elements Os through Bi and their respective isotopic distribution curves.

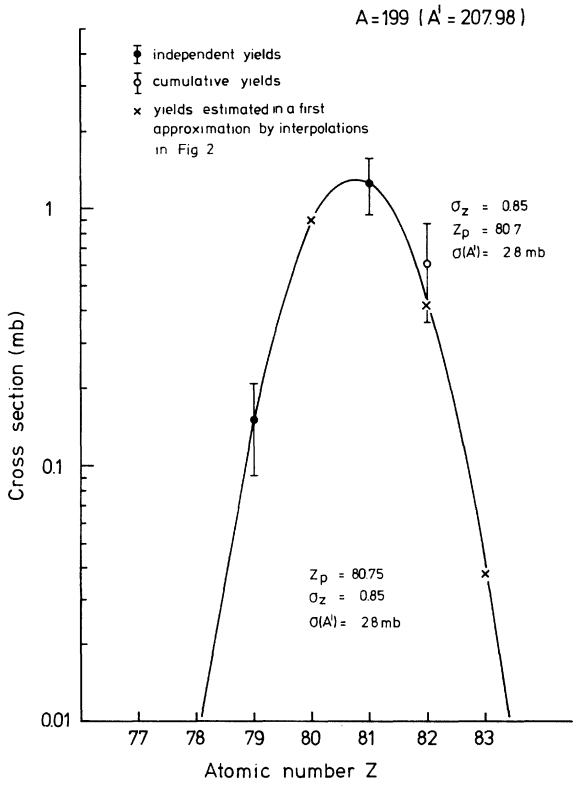

FIG. 3. Charge dispersion curve and parameters [according to Eq. (2)] for the mass chain $A=199$.

TABLE II. Charge and mass distribution for complete fusion-fission in the reaction of 288 MeV ^{40}Ar ions with thick ^{238}U targets.

Product mass number A	Fragment mass number A'	Charge distribution This work Z_p [b]	This work σ_z [c]	Ref. 22 [a] A'	Ref. 22 σ_z	Mass distribution This work	Ref. 22
70	73.15	29.85	0.85				
80	83.61	33.95	0.87				
90	94.06	38.05	0.93			$\sigma_{P_A}=35\pm4$	31
100	104.51	42.1	1.0				
110	114.96	46.15	1.06			$\nu=12\pm1$	11
120	125.41	50.05	1.08				
130	135.86	53.95	1.15				
140	146.32	57.85	1.12	~144	1.19 ± 0.3		
150	156.77	61.65	1.05	~152	1.16		
160	167.22	65.5	1.0				
170	177.67	69.35	0.98				
180	188.12	73.3	0.90				
190	198.57	77.25	0.87	~205	0.95		
200	209.02	81.20	0.85	~209	0.91		
210	219.47			~218	0.81		

[a] Results from 270 MeV ^{40}Ar incident on a thick ^{238}U target; the σ_z values are extracted from five data points in a $2\sigma_z^2$ vs A_1'/A_2' diagram.

[b] Z_p: Most probable charge for a given fragment mass A'; uncertainties in Z_p estimated to be ≤ 0.4.

[c] σ_z: Width parameter for the Gaussian charge dispersion curve; uncertainties in σ_z of the order of ±0.2.

to Z_p, whereas for $|Z - Z_p| > 1.5$ it does not exceed 10–15 %.

Figure 2 shows as an example a set of isotopic distributions vs product mass number for elements with $75 \leq Z \leq 83$; i.e., in a region where only the fusion-fission component is present. Note that the curves drawn in Fig. 2 deviate from those according to Eq. (3) by the just mentioned simplifications. The exact charge dispersion description according to Eq. (2) is used in Fig. 3 to represent the charge dispersion for product mass number 199 (fragment mass number 207.98 for $\nu = 12$). The crosses in Fig. 3 represent yields estimated by interpolations in Fig. 2. The width parameter $\sigma_z = 0.85$ of the fitted Gaussian in Fig. 3 has been determined by least-squares methods from charge dispersion curves for the product masses 196–204. For the variation of σ_z with A' for the fusion-fission distribution, see Table II.

Charge dispersion in the more complicated mass regions near $A = 90$ and $A = 130$ [see Fig. 1(b)] is illustrated by the isotopic yield distributions for yttrium isotopes ($Z = 39$) and iodine isotopes ($Z = 53$) which are shown in Fig. 4. These yields cannot be approximated by a single-component Gaussian charge dispersion curve: the excess yield of neutron-rich isotopes, even though being partially or completely cumulative, cannot be explained in terms of the fusion-fission dispersion curves indicated by solid lines in Fig. 4. These cross sections as well as large portions of the yields of ^{93}Y, ^{99}Mo, ^{103}Ru, ^{105}Ru, ^{107}Rh, ^{139}Ba, ^{140}Ba, ^{141}Ce, ^{142}La, ^{143}Ce, ^{149}Nd, and others have to be assigned to an additional, neutron-rich product distribution superimposed on the fusion-fission distribution. This neutron-rich distribution is interpreted as the result of fission after transfer of a few nucleons and small amounts of excitation energy to the ^{238}U target nuclei. To verify this interpretation, we bombarded a Pb target with ^{84}Kr ions, which cause the same transfer-induced fission as ^{40}Ar.[14,24] Lead isotopes have much higher fission barriers than uranium. Thus, Pb fission should not occur after the transfer of a few nucleons to the target, and the measured iodine isotopic distribution shows that the neutron-rich component was missing.

C. Mass distributions

Plots similar to those presented in Figs. 2–4 have been prepared for the entire mass region $24 \leq A \leq 240$. Only smooth, continuous variations in the charge dispersion parameters and continuous functions P_A were allowed. The various components contributing to the overall mass distribution were then separated from the most abundant component (A) in Fig. 1(b), according to their occurrence in different mass regions, on the basis of

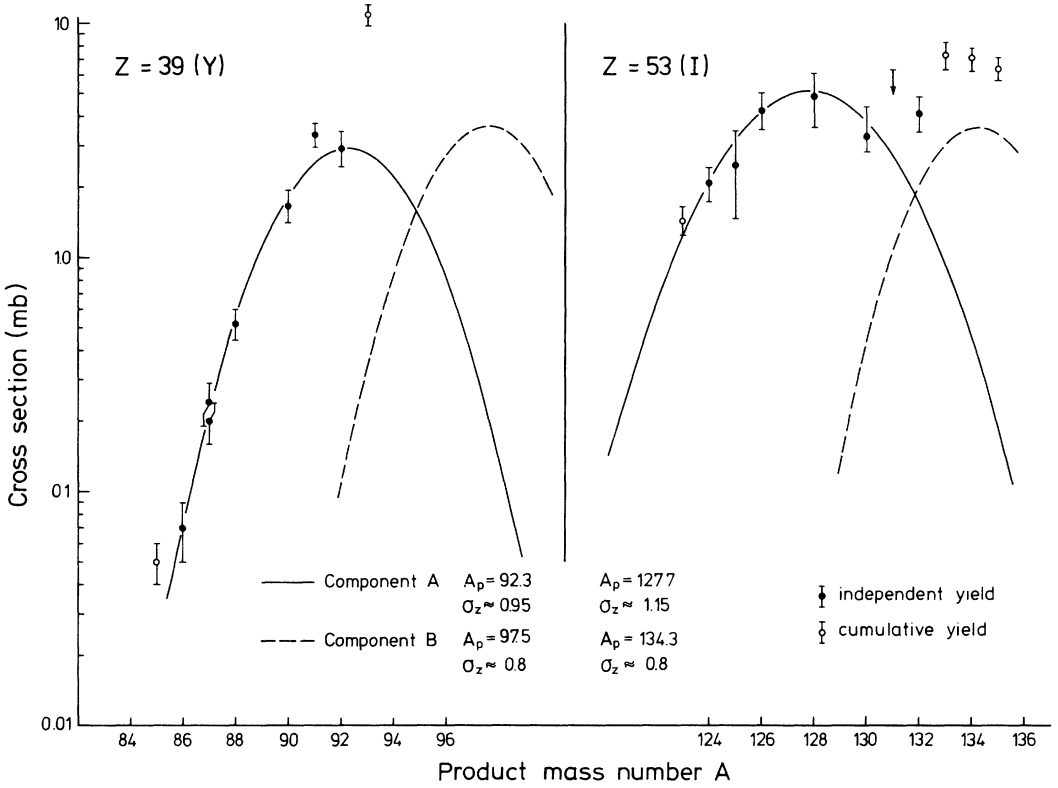

FIG. 4. Isotopic distribution for yttrium and iodine. The solid curves represent the isotopic distribution curves for component A (fusion-fission) fitted with the parameters given in Table II. The dashed curves represent the isotopic distributions for component B (double-humped transfer-induced fission).

their different charge dispersions, and by assuming a Gaussian shape for the mass distribution P_A of the fusion-fission component. The last assumption is derived from the following arguments. It is known that in heavy-ion-induced fission symmetric mass distributions[25-27] in agreement with theoretical predictions[28] are associated with triangular contour plots of fragment mass vs fragment total kinetic energy.[29] Because the typical triangular appearance of fragment mass vs total kinetic energy was observed for fission after full momentum transfer for the $^{40}Ar + ^{238}U$ system,[5,30] the assumption of a symmetric Gaussian mass distribution for this reaction channel seems to be appropriate.

In the following we discuss details relevant for the determination of the mass distributions and integral cross sections of the various components.

1. Complete fusion-fission

The mass distribution function P_A and the integral cross section for complete fusion-fission were calculated with the assumptions about neutron evaporation and charge dispersion discussed in the preceding section. The relevant parameters ν and σ_z were defined in Eqs. (1) and (2). The dependence of the most probable nuclear charge Z_p on the fragment mass A' was treated (1) empirically and (2) with a fixed Z_p function according to the usual charge dispersion hypotheses. This is discussed in more detail in Sec. IV D. In the first case, empirical A_p values were first determined from isotopic distributions for which more than one independent yield was measured (Sc, Zn, Br, Rb, Y, Ag, I, Cs, Tb, Dy, Er, Tm, Ir, Au, Tl, Pb, and Bi). The other dispersion curves were then interpolated with the requirement that the A_p values of adjacent isotopic distributions must be separated by approximately 2.4 mass units. This value is estimated from the mass to charge ratio of the composite system together with appropriate assumptions on the prompt neutron evaporation according to Eq. (1). Successive approximations were used to obtain an empirical set of Z_p values as a function of A'.

This set of Z_p values or one of the fixed Z_p functions was used in a three-dimensional iterative procedure (code MASS) developed to determine the free parameters $\nu, \sigma_z(A')$ and the parameters defining the Gaussian mass distribution function P_A. Another input to this least-squares procedure was

the cross-section data for isotopes assigned to the fusion-fission component on the basis of the plotted isotopic distributions.

If one excludes the yields of neutron-rich isotopes with mass number $80 \leq A \leq 150$ and the Ag, Pd, and Cd cross sections for reasons given below, the fissioning nucleus is calculated to be close to $^{278}_{110}X$ with $\nu = 12$, as expected. The smallest overall error in the computations is obtained when the empirical set of Z_p values is inserted. The calculated fusion-fission cross section is of the order of 500 to 550 mb, depending somewhat on the Z_p function used in the calculation, and the width of the Gaussian mass distribution curve is close to $\sigma_{P_A} = 35$. Also, it is found that the charge dispersion curves are widest for symmetric mass divisions, and the widths decrease with increasing mass asymmetry. In Table II the results are summarized and compared with the results of an earlier radiochemical investigation by Karamyan *et al.*[22] where the charge and mass distribution parameters were extracted from a considerably smaller number of measured cross sections.

The post-neutron emission mass yield curve for the fusion-fission reaction resulting from the data in Table II is shown in Fig. 5 (component A). Its integrated cross section is 525 ± 80 mb.

This cross section is probably slightly low because the experimental technique is not sensitive to fission fragments which escape from the target into the backward hemisphere. We have performed a kinematic calculation on the $^{40}Ar + ^{238}U$ system in the energy interval 288 MeV $\geq E \geq$ 200 MeV, where the velocities of the fragments were derived from their measured energies.[30,31] Also, the finite thickness of the target and the related stopping powers[15] for fission fragments with different masses were taken into account. This calculation shows that for fragments with mass numbers $A' = 200$, $A' = 139$, $A' = 100$, and $A' = 40$ the losses, averaged over the whole energy interval and target thickness, are 10%, 20%, 30%, and 40%, respectively. In our least-squares determination of the mass distribution parameters, the majority of measured cross sections refer to isotopes with $A' > 120$. Thus a correction to the integral cross section for fusion-fission of the order of 10 to 20% is considered appropriate. This correction results in a complete fusion-fission cross section value of 620 ± 150 mb.

2. *Transfer-induced fission*

Using the parameters given in Table II we have calculated independent yields and cumulative yields for a pure fusion-fission product distribu-

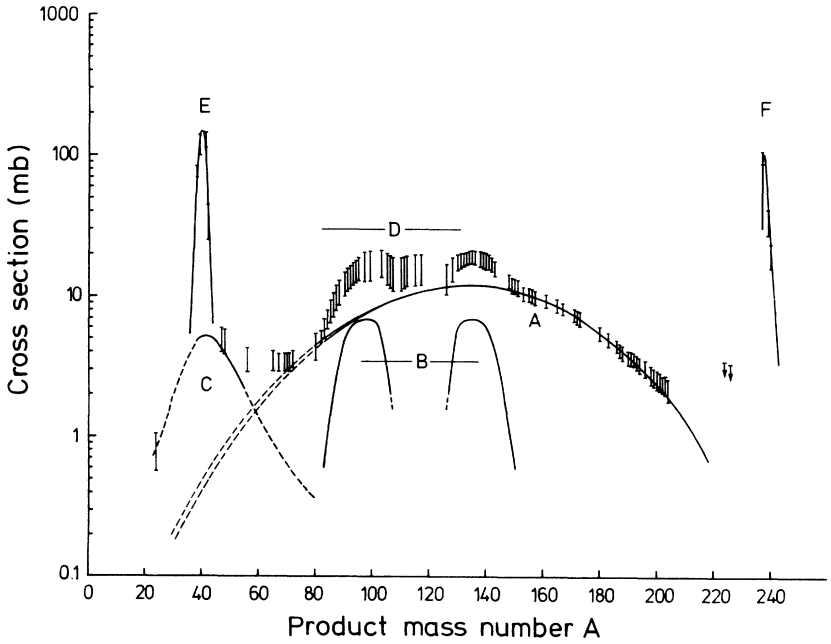

FIG. 5. Total integrated mass yields (upper and lower limits are indicated at those mass numbers for which experimental data were obtained) and their decomposition into individual components: (A) complete fusion-fission, (B) transfer-induced fission, (C) deep inelastic transfer, (E) and (F) quasielastic transfer ("rabbit ears"). The existence of products from the sequential fission of heavy fragments formed in deep inelastic collisions (D) is also indicated; however, we are unable to deduce a mass distribution for this component.

tion and have subtracted these calculated cross sections from the measured data. From the residual cross sections of the neutron-rich isotopes with $80 \leq A \leq 150$ one can then estimate charge- and mass-distribution characteristics for the low-energy transfer-induced fission channel [component B in Fig. 1(b) and Fig. 5] and its integral cross section. This part of the evaluation is described in more detail in a forthcoming paper[14] for the system $^{84}Kr + ^{238}U$, where the same component was observed with characteristics that do not differ within the experimental uncertainties from the $^{40}Ar + ^{238}U$ case. With a constant $\sigma_z = 0.8$ and $\nu \sim 4$ one obtains a double-humped mass distribution similar to those known for low-energy fission at excitation energies of the fissioning nucleus of about 15–20 MeV. The corresponding mass distribution curve is indicated in Fig. 5 (component B). The integral cross section for component B is 150 ± 30 mb, which is lower than the amount of low-energy transfer-induced fission that one would estimate from the difference in cross section between the heavy "rabbit ear" (component F, ~220 mb) and its light complement (component E, ~400 mb). The discrepancy may arise because in a grazing collision the heavy fragment will receive very little forward momentum so that close to 50% of the fission fragments would be emitted into the backward hemisphere and leave the target. The loss is expected to be <50% because a thick target was used. The subtraction of calculated cross sections for isotopes formed in the fusion-fission reaction from the experimental cross sections resulted in another region of residual cross sections which is indicated in Fig. 1(b) as shaded area (component D). These are, in particular, the cross sections of ^{106}Ag, ^{111}Ag, ^{112}Ag, ^{112}Pd, ^{115}Cd, and ^{117}Cd. From the charge to mass ratios of these products it is evident that they cannot be attributed to the just mentioned low-energy transfer-induced fission. By analogy with the $^{84}Kr + ^{238}U$ system, where we observed massive cross sections for these and other isotopes in this mass region originating from the sequential fission of the highly excited "quasi-U" fragments,[14,24] we conclude that the excessive yields of the Ag, Pd, and Cd isotopes have to be attributed to fission after deep inelastic collisions. We are unable to deduce a cross section for this fission process from the few measured yields; however, a rough estimate indicates that a substantial fraction of the heavy products from deep inelastic processes undergoes fission (as discussed in the next section).

3. *Quasielastic transfer and multinucleon transfer*

The delineation of products formed in quasielastic transfer and deep inelastic multinucleon transfer reactions should be made on the grounds of kinetic energy determinations because fragment kinetic energy is the most important parameter characterizing transfer reactions from strongly damped collisions. Distinguishing the reaction products on the basis of different mass distributions alone is difficult.[32] However, it has been shown by Thompson *et al.*[33] and Jacmart *et al.*[34] that the cross sections as a function of Z for light products formed in deep inelastic collisions of ^{40}Ar ions form broad distributions around the nuclear charge of the projectile rather than exhibiting a pronounced peak at $Z = 18$. On the other hand, it is evident from the work by Arthuk *et al.*[10,12] that quasielastic transfer in the $^{40}Ar + ^{232}Th$ reaction is largely restricted to the stripping or pickup of ≤2 protons and a few neutrons while deep inelastic processes are the main mechanism for the formation of reaction products as a result of the transfer of ≥2 protons.

In the present work, the cross sections of products formed by no more than a two-proton transfer such as ^{38}S, ^{38}Cl, ^{39}Cl, ^{41}Ar, ^{237}U, ^{239}U, ^{238}Np, and ^{239}Np have been found to be several tens to hundreds times higher than the yields of products such as ^{24}Na, ^{47}Sc, ^{48}Sc, ^{56}Mn and ^{61}Co, as well as ^{224}Ac and ^{226}Ac which are formed as a result of multinucleon transfer reactions. Although it is possible to fit the yields of the S, Cl, Ar, U, and Np isotopes with very narrow isotopic distribution curves [full width at half maximum (FWHM) ~2, see Fig. 6], the dispersion in A for elements with Z differing by more than two units from $Z = 18$ is more than twice as wide (FWHM = 4–5, see Fig. 7). The number of measured cross sections leaves much to be desired. Therefore, the locations and shapes of the isotopic distribution curves in Figs. 6 and 7 are very rough estimates. However, it can be concluded from the data that the mass distributions for quasielastic and deep inelastic transfer are sufficiently different to allow the differentiation of the two processes in this work.

The width of the curves shown in Fig. 6 is the same as observed in the $^{84}Kr + ^{238}U$ reaction[24] where more data are available. The S, Cl, Ar, and K yields seem to indicate that in the quasielastic transfer protons are preferentially transferred from the projectile to the target. The comparison of estimated cross sections for the formation of complementary elements (K-Pa, Ar-U, Cl-Np, S-Pu) as indicated in Fig. 6 shows that transfer-induced fission becomes increasingly important as the number of nucleons transferred to the target nucleus increases. The integral cross sections for component E(~400 mb) and component F (~220 mb) are estimated to be accurate to ±30%.

The inset in Fig. 7 shows the cross sections for

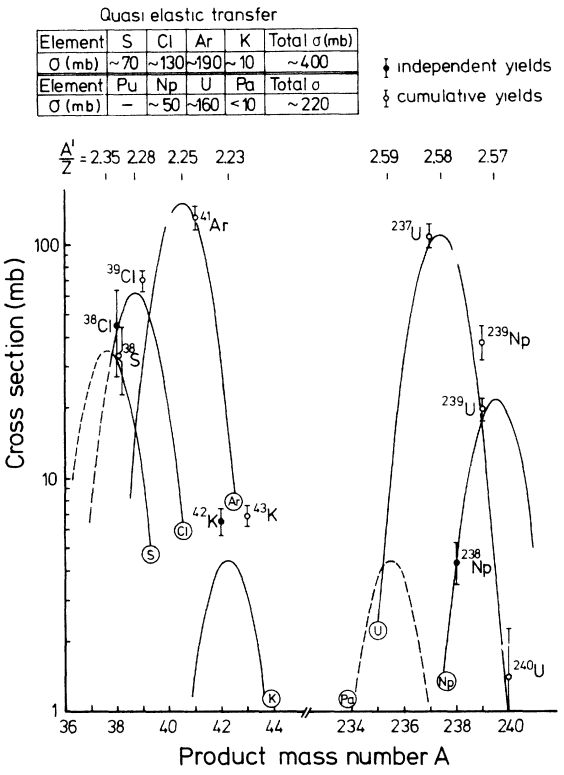

FIG. 6. Cross sections for quasielastic transfer products. The isotopic distribution curves are fitted to the data after subtraction of the contribution from deep inelastic transfer. Total element yields and the most probable mass to charge ratios are also given.

the formation of transfer products (quasielastic plus deep inelastic) in the $^{40}Ar+^{232}Th$ reaction at 388 MeV as a function of the atomic number as given by Arthuk *et al.*[12] A distinction between quasielastic and deep inelastic transfer on the basis of their different mass number distribution, as discussed above, would assign most of the Ar, Cl, and S yield to the quasielastic transfer. Then an almost symmetric distribution remains for the deep inelastic transfer products with a flat maximum near $Z \sim 17$ as indicated by the dashed curve in the inset of Fig. 7. In the main diagram in Fig. 7 we combined this information with our experimental data. In doing this, we neglect the slight odd-even effect favoring the formation of even-Z fragments in the multinucleon transfer processes.[10,12,34] For the purpose of the following estimates, this is certainly satisfactory. For mass numbers $A > 70$ ($Z \geq 30$) our measured cross sections are successfully fitted with the parameters describing the complete fusion-fission distribution. The continuation of the isotopic distribution curves towards lower mass numbers in Fig. 7 is reasonably well defined by the cumulative yields of ^{67}Cu, ^{65}Ni, ^{61}Co, and ^{56}Mn. Note that there is no break in the $Z_p(A')$ systematics in going from a mass region where fusion-fission dominates to masses preferentially formed in deep inelastic direct processes. The curves for $12 \leq Z \leq 19$ are rough estimates based on the cross-section systematics shown in the inset of Fig. 7. The dotted curve in Fig. 7 indicates the integrated mass

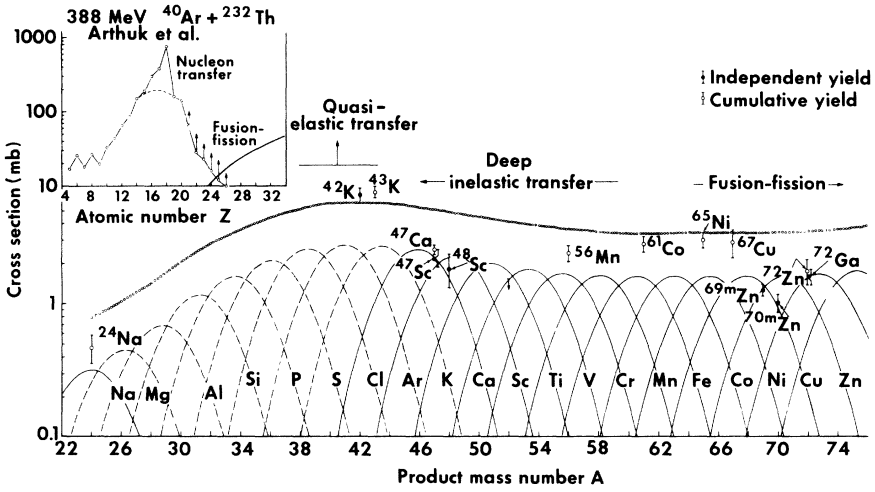

FIG. 7. Isotopic distribution curves for light products ($Z \leq 31$). Cross sections for isotopes produced preferentially by quasielastic transfer are shown separately in Fig. 6. The dotted curve represents the mass yield distribution for deep inelastic transfer plus fusion-fission. Inset: Cross sections for light Z elements formed in quasielastic and deep inelastic processes (from Ref. 12). Our estimate for a division of σ_{dir} into $\sigma_{q.e.t.}$ and $\sigma_{d.i.t.}$ is indicated by the dashed curve (see text).

yields $\sigma(A)$. By subtracting the post-neutron emission mass distribution curve for the fusion-fission component (see Fig. 5) from this curve, we obtain our estimate for the mass distribution of multinucleon transfer products (indicated by the component C curve in Fig. 5). This estimate corresponds to a total cross section for deep inelastic transfer of ~100 mb.

The complementary heavy product distribution was not detected in this work for two reasons. Firstly, the paucity of data points between $A = 204$ $A = 224$ is due to experimental difficulties in detecting the short-lived isotopes in this mass region with the chemical techniques applied in this work. Secondly, it is expected that substantial parts of the heavy transfer products undergo fission, which may be indicated by the excessive Ag, Pd, and Cd cross sections mentioned above. From the shape of the mass distribution curve of component C as reflected to $A = 238$, together with the assumption of neutron evaporation according to Eq. (1) with $\nu = 12$, one can estimate that the contribution of deep inelastic transfer products—were they not to fission—is 16% for $A = 200$ and 6% for $A = 190$. The yields of ^{203,204}Bi and the cumulative yields of the neutron-deficient Pb isotopes, which are slightly high when compared with the calculated fusion-fission cross sections, may indicate the presence of surviving multinucleon transfer (deep inelastic) products.

D. Z_p function for fusion-fission and deep inelastic transfer

Empirical Z_p values for a few mass number chains are listed in Table II. As mentioned above, these Z_p values describe the data better than any of the usual charge distribution hypotheses on the basis of smaller overall errors obtained in the calculations. Also, it was mentioned that there is no break in the mass to charge ratios if one leaves the mass region dominated by fusion-fission and enters the deep inelastic transfer region. Here A'/Z ratios of about 2.4 are observed, the A'/Z ratios of the composite system being 2.53. This result is in agreement with Ref. 10, and with results obtained at Orsay.[35] Apparently, the mass to charge ratio of the composite system plays a dominant role in the determination of this ratio for the fragments. This implies that the mass to charge ratio degree of freedom, which is known to be equilibrated in the fusion-fission process, is already equilibrated in deep inelastic collisions; i.e., has a relaxation time short compared to the lifetime of the double-nucleus structure[10] in deep inelastic collisions. On the other hand, our data indicate that equilibration is not reached in the quasielastic transfer where A'/Z ratios of ~2.25 and ~2.58 are observed, for the light A and heavy A components, respectively, which are close to those of projectile and target. These ratios are calculated with the assumption that no particles are evaporated from the transfer products. This is proven for the light fragments[34]; also, the heavy transfer products observed in this work are most likely formed with excitation energies too low for particle evaporation, because at higher excitation energies fission would compete strongly with particle evaporation.

Proposals regarding the charge distribution in fission have been available since 1947. The empirically determined Z_p values for deep inelastic transfer products and for fusion-fission products are compared in Fig. 8(a) with the predictions of the three main recipes which are in general use: (1) Unchanged charge density (UCD). This hypoth-

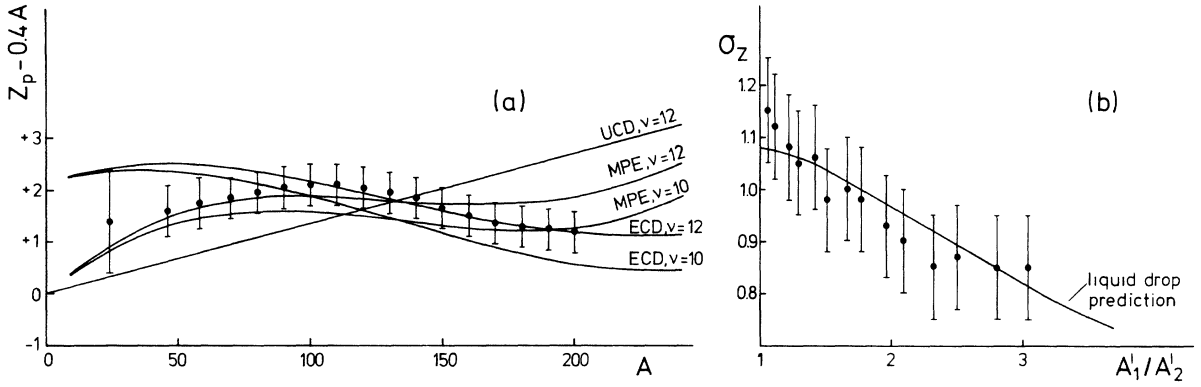

FIG. 8. (a) Comparison of experimentally determined Z_p values for fusion-fission products and products from deep inelastic transfer with predictions according to the UCD, MPE, and ECD hypotheses (see text). (b) Dependence of the width parameter σ_z of the charge dispersion for fusion-fission on the ratio of the fragment masses. The curve indicates the shape of the liquid drop prediction.

esis assumes that the composite nucleus (Z_0, A_0) fissions so rapidly that the fragments would both have the same neutron-to-proton ratio and

$$Z_p = A' \frac{Z_0}{A_0} = A \frac{Z_0}{A_0 - \nu}. \tag{4}$$

The UCD assumption corresponds to straight lines with different slopes for different ν values in a Z_p-0.4A vs A diagram [see Fig. 8(a)].

(2) Equal charge displacement (ECD). This hypothesis proposes that the Z_p values of the fission fragment and its complement be an equal number of units away from the line of β stability:

$$|Z_p(A_1') - Z_\beta(A_1')| = |Z_p(A_2') - Z_\beta(A_2')|, \tag{5}$$

where $Z_\beta(A')$, i.e., the charge that corresponds to β stability, is calculated from the Myers-Swiatecki mass formula.[36] The resulting $Z_p - 0.4$ vs A curves for $\nu = 10$ and $\nu = 12$ are plotted in Fig. 8(a).

(3) The minimum potential energy (MPE) postulate proposes a distribution of charge such that a minimum is obtained for the potential energy (including Coulomb repulsion) of the two touching fragments. In the absence of shell effects Swiatecki[37] has given an approximation for two tangent spheres of radii R_1, R_2:

$$Z_p = A' \frac{Z_0}{A_0}\left[1 + 0.005 A_0^{2/3} F\left(\frac{R_1}{R_2}\right)\right], \tag{6}$$

where F is the following function:

$$F(\lambda) = (0.2 + 1.2\lambda - 1.2\lambda^2 - 0.2\lambda^3)/(1+\lambda)(1+\lambda^3)^{5/3}$$

and $\lambda = R_1/R_2$. The respective curves for $\nu = 10$ and $\nu = 12$ are plotted in Fig. 8(a).

A minimization of the sum of potential energy and Coulombic repulsion using the Myers-Swiatecki mass formula (which thus includes shell effects for two separated fragments) gives $Z_p - 0.4A$ vs A curves that are similar to the ones obtained from Swiatecki's MPE approximation; however, their agreement with the experimental data is somewhat worse.

Figure 8(a) shows that the UCD prediction is not in agreement with the experimental findings. The s-shaped pattern of the data is reasonably reproduced by the MPE approximation with $\nu = 12$ for the masses $A \leq 150$ or by ECD prediction with $\nu = 12$ for masses $A \geq 100$. Both predictions deviate from the data for light (ECD) or heavy (MPE) masses. The general disagreement of the experimental dependence $Z_p - 0.4A$ vs A with the UCD prediction and, on the other hand, the proximity of the data to both ECD and MPE predictions signify that the time necessary to equilibrate the mass to charge ratios of the fragments originating from fusion-fission and from deep inelastic transfer is short compared to the lifetime of the composite system.

The use of a liquid drop formula to describe the potential energy E of two touching fragments allows us also to predict the dependence of the charge dispersion width parameter σ_z as a function of A'. In a first approximation σ_z is given as

$$\sigma_z \approx 1 \Big/ \frac{\partial^2 E}{\partial Z_1^2} = \text{const}\left[A_1'\left(1 - \frac{A_1'}{A_0}\right)\right]. \tag{7}$$

This relation[37] has a maximum at $A' = \frac{1}{2}A_0$ which is in agreement with experiment (see Table II). In Fig. 8(b) the experimentally observed dependence σ_z vs A_1'/A_2' is compared to the functional form of this dependence (not its absolute magnitude) as predicted by a version of Eq. (7) which includes higher order terms. The agreement is reasonable for asymmetric mass splits. A systematic deviation to higher σ_z values is indicated for the nearly symmetric mass splits. Most likely this deviation is the result of a contribution of component D to σ_z of the fusion-fission component in this mass region, which we did not attempt to take into account. Karamyan *et al.*[22] compared the absolute magnitude of σ_z to the prediction of the statistical theory of fission. Due to the disagreement between experiment and theory, it was concluded that an additional charge variance originating from the finite dimensions of the neck joining the fission fragments at the instant of fission has to be assumed.[38]

V. ANGULAR MOMENTA INFERENCES

The thick target cross sections of this work can be associated with an effective energy (see Appendix A). It is then possible to compare the cross sections obtained in this work with the previously reported results on the $^{40}Ar + ^{238}U$ system by Hanappe *et al.*,[5] Nguyen Tac Anh *et al.*,[39] and Sikkeland[11] and the results on the very similar system $^{40}Ar + ^{232}Th$ by Arthuk *et al.*[10,12] In the following, the $^{40}Ar + ^{232}Th$ system is treated as if the target had been ^{238}U; the differences in the barriers and radii are considered small enough to ignore for the purpose of the following discussion. Table III summarizes the available data. Except for the measured total reaction cross section of this work, the σ_r values are estimated by using the relation

$$\sigma_r = \pi R^2\left(1 - \frac{B}{E}\right), \tag{8}$$

where $R = r_{\text{eff}}(A_1^{1/3} + A_2^{1/3})$ with $r_{\text{eff}} = 1.44$ fm, $B = 171$ MeV[11,21] in the center of mass system. r_{eff} values determined and extrapolated from elastic scattering data using the one-quarter point technique are close to 1.41 fm (Ref. 32); however, a slightly larger radius would be more consistent with the fact that at the one-quarter point of

TABLE III. Summary of measured cross sections in the $^{40}Ar + ^{238}U$ (^{232}Th) system, deduced angular momentum limits, and comparison with theoretical predictions.

Ref.	E_{lab} (MeV)	$E_{c.m.}$ (MeV)	$\sigma_{fus\text{-}fiss}$ (mb)	σ_{dir} (mb)	$\sigma_{q.e.t.}$ (mb)	$\sigma_{d.i.t.}$ (mb)	σ_r [a] (mb)	$\pi\lambda^2$ (mb)	l_{max} [b] ($\hbar$ units)	l_{crit} [c] ($\hbar$ units)	Rotating liquid drop model $J_{B_f}=0$	Bass J(limit) ($f=\frac{5}{7}$)
This work	200–288	171–247	620	500	400	100	1120 [d]	0.09177	108	81		
5	250	214	766 [e]				1210	0.08965	115	91		
39	270	231	950				1570	0.08298	137	106		
10,12	297	253	(850) [f]	1100	525 [g]	575 [g]	1950	0.07581	159	(105)	0	147
5	300	257	1220 [e]				2020	0.07470	163	127		
10,12	388	331	(360) [f]	2560	800 [g]	1760 [g]	2920	0.05795	223	(78)		
11	416	356	1330				3140	0.05388	240	156		

[a] The σ_r value from this work is obtained experimentally for a thick target as $\sigma_r = \sigma_{fus\text{-}fiss} + \sigma_{q.e.t.} + \sigma_{d.i.t.}$. The other values are calculated for thin targets with $r_{eff} = 1.44$ fm.

[b] Calculated from $\sigma_r = \pi\lambda^2(l_{max}+1)^2$.

[c] Calculated from $\sigma_{fus\text{-}fiss} = \pi\lambda^2(l_{crit}+1)^2$.

[d] See Appendix A (iii).

[e] According to recent angular distribution measurements by Tamain *et al.* (Ref. 40) these values are slightly overestimated.

[f] Obtained as $\sigma_r - \sigma_{dir}$.

[g] Division of σ_{dir} into $\sigma_{q.e.t.}$ and $\sigma_{d.i.t.}$ performed on the basis of their different mass distributions (see text).

$\sigma_{el}/\sigma_{Ruth}$ one usually already observes a sizeable cross section for quasielastic transfer reactions. The value $r_{eff} = 1.44$ fm was proposed by Oganessian *et al.*[21]

As discussed in Sec. IV C and illustrated in the insert of Fig. 7, we have made estimates on how to divide σ_{dir} [10,12] at 297 and 388 MeV into their quasielastic and deep inelastic components on the basis of their different mass distributions. Our estimates are included in Table III. The $\sigma_{q.e.t.}$ values indicate that at low energies quasielastic transfer is an important part of σ_r, while its relative cross section $\sigma_{q.e.t.}/\sigma_r$ decreases for higher energies to $\leq 25\%$. On the other hand, the deep inelastic direct component is of little importance at low energies. According to Refs. 10 and 12 its importance increases substantially with increasing energy.

While the σ_{dir} at 297 MeV [10] may still be considered as consistent with the $\sigma_{fus\text{-}fiss}$ data at 270 MeV [39] and 300 MeV,[5] especially if one keeps in mind that the 300 MeV fusion-fission cross section is probably slightly overestimated,[40] the direct reaction cross section σ_{dir} at 388 MeV [10,12] and the fusion-fission cross section measured by Sikkeland[11] at 416 MeV are clearly inconsistent. One can think of arguments which modify the interpretation of both these experiments: for example, Arthuk *et al.*[10,12] may have underestimated the width σ_{P_A} of the fusion-fission mass distribution, which should be very large at 388 MeV. This would imply that part of the light fragments detected in their work were fusion-fission fragments. On the other hand, Sikkeland's fusion-fission cross section might be high because it may include contributions from deep inelastic collisions, which also occur after full momentum transfer from the projectile to the combined system. Also, Sikkeland's assumption that the total binary fission cross section observed in his experiments is equal to the total reaction cross section needs to be reexamined.

Despite the serious uncertainties in $\sigma_{fus\text{-}fiss}$ at high energies we would like to conclude with a remark related to the limiting angular momentum values l_{crit} in Table III and their energy dependence.

First, we would like to compare these results with the predictions by the rotating liquid drop model[41] which has been successful in reproducing evaporation residue cross sections for light systems if fission competition in the deexcitation of the compound nucleus is included. In this model the limiting value l_{crit} is obtained from the condition that the fission barrier vanishes ($B_f = 0$) for a particular J value above which a compound nucleus should not exist. The prediction for $^{40}Ar + ^{238}U$ is that $B_f = 0$ even for the lowest partial waves and that no compound nucleus should be formed. If this prediction has a physical significance, one might expect that the fission events observed in $^{40}Ar + ^{238}U$ (and in lighter systems at higher energies) are distinct from fission of angular momentum states with definite fission barriers. How-

ever, there is no experimental evidence for such a distinction. The fission events above $B_f = 0$ have the same characteristics as fission from an equilibrated compound nucleus: $1/\sin\theta$ angular distributions,[40,42] triangular shaped fragment mass vs fragment total kinetic energy contours,[29] and symmetric mass distributions with equilibrated mass to charge ratios (this work). The discrepancies between the experimental fusion-fission cross sections and the rotating liquid drop model predictions may be connected with the sharp-cutoff approximation at $B_f = 0$.[29]

The Bass model,[43] where the limitations of $\sigma_{\text{fus-fiss}}$ are derived from a static interaction configuration, has been quite successful in reproducing fusion cross sections including cross sections for fusion-fission. In particular, this model reproduces well the general observation that l_{crit} *increases* with increasing center of mass energies. This model predicts a saturation at a maximum value of l_{crit} for the highest energies. Figure 9 shows the prediction of the Bass model together with the experimental l_{crit}^2 values from Table III. In contrast to the model prediction and in contrast to a large body of other fusion and fusion-fission data for systems up to $^{40}\text{Ar} + ^{165}\text{Ho}$,[1] the l_{crit} values derived from the results by Arthuk *et al.*[10,12] would indicate a marked decrease of l_{crit} at higher center of mass energies. If this trend is corroborated by new measurements, this could be the first evidence that the fission process in a case like

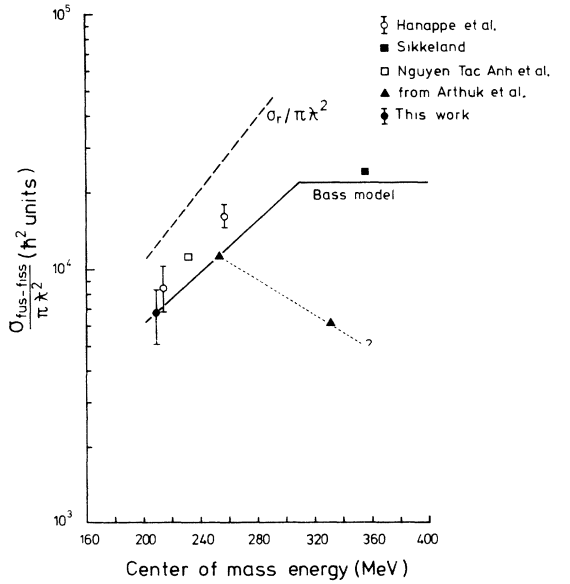

FIG. 9. Comparison between experimental and calculated values of l_{crit} as a function of the bombarding energy. The experimental results are shown by the points. The prediction by the Bass model (Ref. 43) is indicated as a solid line.

$^{40}\text{Ar} + ^{238}\text{U}$ is distinct from fission of a compound nucleus insofar as the energy dependence of its limiting orbital angular momenta is different from that for compound nucleus fission.

VI. SUMMARY

The results obtained from this survey experiment can be summarized as follows:

(1) In the energy interval investigated fusion-fission accounts for about 55% of the total reaction cross section, while 35% quasielastic and 10% deep inelastic transfer are observed. The mass distributions of these components are shown in Fig. 5. The total reaction cross section amounts to about 1100 mb.

(2) Evidence is presented for fission of heavy nuclei after transfer reactions. Quasielastic transfer leads to a double-humped fission product distribution signifying the transfer of relatively small amounts of excitation energy in grazing collisions. Fission after deep inelastic collisions seems to lead to a fission fragment mass distribution which is typical for higher excitation energies of the fissioning nucleus.

(3) Proton pickup reactions are observed leading to a buildup of products with $Z \geq 26$; i.e., the mass distribution for multinucleon transfer and fusion-fission overlap considerably.

(4) It is shown that the mass to charge ratios for both multinucleon transfer and fusion-fission fragments are equilibrated. No equilibration of this degree of freedom is attained for products formed by quasielastic transfer.

(5) The l_{crit} value derived from this work is consistent with the prediction of the Bass model.

APPENDIX A. CALCULATION OF CROSS SECTIONS FROM A THICK TARGET EXPOSURE

(i) The thick target cross section for a given radioactive reaction product was calculated from its absolute decay rate R_0 at the end of bombardment as

$$\sigma = \frac{R_0}{(1 - e^{-\lambda t})\phi N_T}\ , \tag{9}$$

where λ is the decay constant, t is the irradiation period, ϕ is the average flux per time unit, and N_T is the number of target atoms per cm^2. Corrections to R_0 are mentioned in Sec. II B.

(ii) As shown by Oganessian *et al.*[21] in the system ^{40}Ar on ^{238}U, there is one general interaction barrier $B_{\text{c.m.}} = 171 \pm 3$ MeV and one general radius parameter $r_{\text{eff}} = 1.44 \pm 0.01$ fm for reaction channels which lead to the formation of ^{237}U, ^{238}Np, lanthanide, and Au nuclides. Thus, in the calcula-

tion of the cross sections for quasielastic transfer, deep inelastic transfer, and fusion-fission in this work, it was not necessary to correct for differences in their energy dependence. In the absence of better knowledge the same approach was applied to calculate the cross section for transfer-induced fission, which, however, is not relevant for the discussion of angular momenta inferences in Sec. V.

For the calculation of N_T, an effective target thickness of 17.3 mg U/cm^2 (deduced from a range table[15] for the energy interval between the interaction barrier and the incident energy) was assumed regardless of the reaction mechanism through which the given product was formed.

(iii) The total reaction cross section obtained in this work (1120 mb, see Table III) is in agreement with the mean geometrical cross section

$$\bar{\sigma}_r = \pi R^2 \frac{\int_B^E (1 - B/E) dE}{E - B} = 1036 \text{ mb}, \qquad (10)$$

where $R = r_{eff}(A_1^{1/3} + A_2^{1/3})$ and $r_{eff} = 1.44$ fm, $B = 171$ MeV, and $E = 247$ MeV. To compare the thick target cross sections of this work with other thin target data, it is necessary to associate an effective energy with the thick target cross sections. With the above mentioned values for the parameters r_{eff}, B, and E the effective energy is

$$E_{eff} = \frac{B}{1 - \bar{\sigma}_r / \pi R^2} = 206.5 \text{ MeV}, \qquad (11)$$

while the experimental value for σ_r correlates with an effective energy of 210 MeV.

APPENDIX B. CHEMICAL SEPARATION OF Au, Tl, AND Y

For the separation of Au, Tl, and Y the uranium target was dissolved in concentrated HNO_3. After addition of 10 mg of Y^{3+} carrier and 50 μg of Au^{3+} carrier as well as a known amount of ^{195}Au tracer activity, the solution was made 2 M in HCl/Cl_2.

Gold and thallium were extracted from the aqueous phase into diethyl ether. The ether was evaporated and the residue dissolved in 0.5 ml of 12 M HCl/Cl_2. This solution was passed through a cation exchange resin (analytical grade AG 50W $\times$8) obtained from Bio-Rad Laboratories, and used in a column of 3 mm inside diameter and 5.0 cm length; this resin absorbs Au and Tl(III). The column was washed with 3 ml of 12 M HCl. Au and Tl(III) were then stripped from the column in 0.5 ml of water and mounted for counting by evaporation. The chemical yield for Au was determined via the amount of tracer activity recovered in the final sample (typically 50–70%). The chemical yield of Tl(III) was obtained by normalizing the cross sections to the previously determined cross sections of ^{199}Tl and ^{201}Tl.

Yttrium was precipitated in the aqueous phase as $Y(OH)_3$. Its further purification procedure involved extraction of Y(III) into a n-heptane solution of di-(2-ethylhexyl)-orthophosphoric acid and a series of precipitations of YF_3, $Y(OH)_3$, and $Y_2(C_2O_3)_3$. Details are described elsewhere.[44] The final $Y_2(C_2O_4)_3$ precipitate was filtered onto a membrane filter and mounted for counting. After completion of the counting, the sample was ashed to Y_2O_3 and weighed to determine the chemical yield for Y (typically 40%). The cross sections of a few heavy lanthanide elements, which accompany yttrium in this separation procedure, were normalized to previously determined cross sections.

ACKNOWLEDGMENTS

The authors wish to thank Dr. A. Ghiorso and Dr. J. M. Nitschke and the staff of the superHILAC for their practical solutions to many problems and for their help in performing the irradiations. The contributions of Miss M. DiCasa and Mr. I. Binder in compiling the γ-ray reference table are gratefully acknowledged. Our thanks are also due Dr. W. Swiatecki and Dr. M. M. Fowler for helpful discussions concerning interpretation of our data. The aluminum-backed U target was kindly supplied by Dr. E. K. Hulet and Dr. W. F. Brunner, Jr. (LLL). Financial support from Gesellschaft für Schwerionenforschung, GSI, Darmstadt, Germany, and from the Swedish Atomic Research Council is much appreciated.

---

†Work supported by the U. S. Energy Research and Development Administration.

*On leave from Institut für Kernchemie, Universität Mainz, Germany. Present address: Gesellschaft für Schwerionenforschung, GSI, Darmstadt, Germany.

‡Department of Nuclear Chemistry, Chalmers University of Technology, Göteborg, Sweden.

§Los Alamos Scientific Laboratory, University of California, Los Alamos, New Mexico 87545.

[1]M. Lefort, Y. Le Beyec, and J. Peter, in *Proceedings of the International Conference on Reactions Between Complex Nuclei, Nashville, June 1974*, edited by R. L. Robinson, F. K. McGowan, J. B. Ball, and J. H. Hamilton(North-Holland, Amsterdam/American Elsevier, New York, 1974), Vol. II, p. 81.

[2]J. B. Natowitz, E. T. Chulik, and M. N. Namboodiri, Phys. Rev. C 6, 2133 (1972).

[3]H. H. Gutbrod, F. Plasil, H. C. Britt, B. Erkkila, R. H. Stokes, and M. Blann, in *Proceedings of the Third Symposium on the Physics and Chemistry of*

Fission, Rochester, 1973 (IAEA, Vienna, 1974), Vol. II, p. 309.
[4]T. Sikkeland, V. E. Viola, and E. L. Haines, Phys. Rev. 125, 1350 (1962).
[5]F. Hanappe, C. Ngô, J. Péter, and B. Tamain, in *Proceedings of the Third Symposium on the Physics and Chemistry of Fission, Rochester, 1973* (see Ref. 3), Vol. II, p. 289.
[6]F. Hanappe, M. Lefort, C. Ngô, J. Péter, and B. Tamain, Phys. Rev. Lett. 32, 738 (1974).
[7]K. L. Wolf, J. P. Unik, J. R. Huizenga, J. Birkelund, H. Freiesleben, and V. E. Viola, Phys. Rev. Lett. 33, 1105 (1974).
[8]J. Péter, C. Ngô, and B. Tamain, J. Phys. Lett. (Paris) 36, L-23 (1975).
[9]A. G. Arthuk, V. V. Avdeichikov, J. Ero, G. F. Gridnev, V. L. Mikheev, and V. V. Volkov, Nucl. Instrum. Methods 83, 72 (1970).
[10]A. G. Arthuk, G. F. Gridnev, V. L. Mikheev, V. V. Volkov, and J. Wilcyński, Nucl. Phys. A215, 91 (1973).
[11]T. Sikkeland, Ark. Fys. 36, 539 (1967); Phys. Lett. 27B, 277 (1968).
[12]A. G. Arthuk, G. F. Gridnev, V. L. Mikheev, and V. V. Volkov, JINR Report No. JINR E7-8590, 1975 (unpublished).
[13]J. V. Kratz, J. O. Liljenzin, A. E. Norris, I. Binder, and G. T. Seaborg, in *Proceedings of the International Conference on Reactions Between Complex Nuclei, Nashville, June 1974* (see Ref. 1), Vol. I, p. 88.
[14]J. V. Kratz, A. E. Norris, and G. T. Seaborg, Phys. Rev. C (to be published).
[15]L. C. Northcliffe and R. I. Schilling, Nucl. Data A7, 233 (1970).
[16]J. V. Kratz, J. O. Liljenzin, and G. T. Seaborg, Inorg. Nucl. Chem. Lett. 10, 951 (1974).
[17]I. Binder, M. DiCasa, J. V. Kratz, J. O. Liljenzin, and A. E. Norris, LBL Annual Report No. LBL-2366, 1973 (unpublished), p. 451.
[18]C. M. Lederer, J. M. Hollander, and I. Perlman, *Tables of Isotopes* (Wiley, New York, 1967), 6th ed.
[19]J. Blachot and R. de Tourreil, J. Radioanal. Chem. 11, 351 (1972).
[20]C. M. Lederer, unpublished data sheets, private communication.
[21]Y. T. Oganessian, Y. E. Penionzhkevich, K. A. A. Gavrilov, and Kim De En, JINR Report No. JINR *P7*-7863, 1974 (unpublished).
[22]S. A. Karamyan, Y. T. Oganessian, Y. E. Penionzhkevich, and B. I. Pustylnik, Yad. Fiz. 9, 715 (1969) [Sov. J. Nucl. Phys. 9, 414 (1969)].
[23]Y. T. Oganessian, in *Proceedings of the Second Symposium on Physics and Chemistry of Fission, Vienna, 1969* (IAEA, Vienna, 1969), p. 489.
[24]J. V. Kratz, A. E. Norris, and G. T. Seaborg, Phys. Rev. Lett. 33, 502 (1974).
[25]F. Plasil, R. L. Ferguson, F. Pleasonton, in *Proceedings of the Third Symposium on the Physics and Chemistry of Fission, Rochester, 1973* (see Ref. 3), Vol. II, p. 319.
[26]F. Plasil, D. S. Burnett, H. C. Britt, and S. G. Thompson, Phys. Rev. 142, 696 (1966).
[27]R. L. Ferguson, F. Plasil, H. Freiesleben, C. E. Bemis, and H. W. Schmitt, Phys. Rev. C 8, 1104 (1973).
[28]J. R. Nix and W. J. Swiatecki, Nucl. Phys. 71, 1 (1965).
[29]F. Plasil, in *Proceedings of the International Conference on Reactions Between Complex Nuclei, Nashville, June 1974* (see Ref. 1), Vol. II, p. 107.
[30]M. Lefort, J. Phys. A 7, 107 (1974).
[31]B. Borderie, F. Hanappe, C. Ngô, J. Péter, and B. Tamain, Nucl. Phys. A220, 93 (1974).
[32]J. R. Huizenga, Institute of Nuclear Research, Warsaw, Poland, Report No. UR-NSRL-90, 1974, Nukleonika. 20, 291 (1975).
[33]S. G. Thompson, L. G. Moretto, R. C. Jared, R. P. Babinet, J. Galin, M. M. Fowler, R. C. Gatti, and J. B. Hunter, Phys. Scr. 10A, 36 (1974).
[34]J. C. Jacmart, P. Colombani, H. Doubre, N. Frascaria, N. Poffé, M. Riou, J. C. Roynette, C. Stéphan, and A. Weidinger, Nucl. Phys. A242, 175 (1975).
[35]B. Gatty, D. Guerreau, M. Lefort, J. Pouthas, X. Tarrago, J. Galin, B. Cauvin, J. Girard, and H. Nifenecker, Institute de Physique Nucleaire, Orsay, Report No. IPNO-RC-74-07, 1975.
[36]W. D. Myers and W. J. Swiatecki, UCRL Report No. UCRL-11980, 1965 (unpublished).
[37]W. J. Swiatecki, J. Phys. (Paris) 33, C5-45 (1972); and private communication.
[38]S. A. Karamyan, Y. T. Oganessian, and B. I. Pustylnik, Yad. Fiz. 11, 982 (1970) [Sov. J. Nucl. Phys. 11, 546 (1970)].
[39]Nguyen Tac Anh, Y. T. Oganessian, and Y. E. Penionzhkevich, in *Proceedings of the International Conference on Reactions Between Complex Nuclei, Nashville, June 1974* (see Ref. 1), Addendum to Vol. I, p. 15.
[40]B. Tamain, C. Ngô, J. Péter, R. Lucas, J. Poitou, and H. Nifenecker, Institut de Physique Nucleaire, Orsay, Report No. IPNO-RC-75-04, 1975 (unpublished).
[41]S. Cohen, F. Plasil and W. J. Swiatecki, Ann. Phys. (N.Y.) 82, 557 (1974); F. Plasil and M. Blann, Phys. Rev. C 11, 508 (1975).
[42]M. Lefort, Institut de Physique Nucleaire, Orsay, Report No. IPNO-RC-74-06, 1974 (unpublished).
[43]R. Bass, Phys. Lett. 47B, 139 (1973).
[44]A. E. Norris, Ph.D. thesis, Washington University, 1963 (unpublished).